Toxicology 444 (2020) 152564

Contents lists available at ScienceDirect

Toxicology

journal homepage: www.elsevier.com/locate/toxicol

In-vitro toxicity of molybdenum trioxide nanoparticles on human keratinocytes

Ksenija Božinović [a,1], Davor Nestić [a,1], Urška Gradišar Centa [b], Andreja Ambriović-Ristov [a], Ana Dekanić [a], Lenn de Bisschop [a], Maja Remškar [b], Dragomira Majhen [a,*]

[a] Laboratory for Cell Biology and Signaling, Division of Molecular Biology, Ruđer Bošković Institute, Bijenička 54, 10000 Zagreb, Croatia
[b] Laboratory for Synthesis of Inorganic nanotubes, Solid State Physics Department, Jožef Stefan Institute, Jamova cesta 39, 1000 Ljubljana, Slovenia

ARTICLE INFO

Keywords:
Nanoparticles
Cell toxicity
MoO_3
Nanotoxicology
Nanomaterial biocompatibility

ABSTRACT

Molybdenum trioxide (MoO_3) nanoparticles (NPs) embedded in polymer films have been proposed as a cheap way of producing antibacterial coatings on external surfaces. Recently, we synthesized MoO_3 nanowires in a unique shape and degree of anisotropy, which enables their fast water dissolution and quick antimicrobial reaction. Potential human health risks following the exposure to MoO_3 NPs however need to be assessed prior their wide use. We therefore, investigated the biological effect of these newly synthesized MoO_3 NPs on the human keratinocyte cell line HaCaT, used here as a model for the human skin. Exposure of HaCaT cells to 1 mg/mL MoO_3 NPs concentration for 1 h showed no effect on cell survival, had no influence on reactive oxygen species production, expression of proteins involved in antioxidant defense, secretion of pro-inflammatory cytokines, nor induced DNA damage. Interestingly however, ERK and p38 MAP kinases were activated, and upon longer time exposure, induced a moderate release of the pro-inflammatory cytokine interleukin 6, increased DNA damage and increased the level of caspase independent cell death. Our study indicates that exposing HaCaT cells to antibacterial MoO_3 NPs water-based solution in durations less than 1 h exhibits no cytotoxicity, but rather triggers cell signalling involved in cell survival and inflammation; which should be taken into consideration when evaluating MoO_3 NPs for medical applications.

1. Introduction

Due to their unique physical and chemical characteristics, nanoparticles have been broadly used in electronics, textile industry, cosmetics, tissue engineering and nanomedicine (Dastjerdi and Montazer 2010; Hasan et al. 2018; Karim et al. 2019; Raj et al. 2012). Recently, metal and metal-oxide-based nanoparticles have gained increased attention in the biomedical field because of their antimicrobial activity, which is evidenced at even very low concentrations (Hajipour et al. 2012). Moreover, it has been shown that most mechanisms involved in antibiotic resistance do not affect antimicrobial activity of nanoparticles (Gold et al. 2018; Wang et al. 2017). Out of the different nanomaterials exhibiting antibacterial properties, MoO_3 in the form of NPs has become very attractive (Zollfrank et al. 2012).

In one study, the antibacterial efficiency of MoO_3 nanoplates was evaluated against four types of pathogens. The minimum inhibitory concentrations of MoO_3 at 8 μg/mL (against *Escherichia coli*, *Salmonella typhimurium* and *Bacillus subtilis*), and 16 μg/mL (against *Enterococcus faecalis*), showed that MoO_3 nanoplates have a predominant antibacterial activity compared to the standard antibiotic, kanamycin (Krishnamoorthy et al. 2013). It was also shown that MoO_3 NPs create an acidic pH and display a universal antimicrobial activity against antibiotic-susceptible and resistant isolates belonging to the most relevant bacterial species responsible for hospital-acquired infections (Lopes et al. 2018).

Hospitalized patients are often immunocompromised and prone to infections, thus finding a permanent solution to prevent accumulation and spread of infectious agents is warranted. Covering the surfaces of susceptible environments with an antimicrobial coating could be a successful way to avoid bacterial growth. For this purposes, MoO_3 NPs can be embedded in films made of different materials (Krishnamoorthy et al. 2014; Picarra et al. 2019).

One of the major concerns regarding medicinal usage of MoO_3 NPs is their biocompatibility. Studied *in vitro*, MoO_3 NPs showed cytotoxic

* Corresponding author.
E-mail address: dragomira.majhen@irb.hr (D. Majhen).
[1] Equally contributed authors.

https://doi.org/10.1016/j.tox.2020.152564
Received 26 June 2020; Received in revised form 14 August 2020; Accepted 22 August 2020
Available online 5 September 2020

effects on rat liver cells (Hussain et al. 2005), along with lung and breast cancer cell lines (Fakhri and Nejad 2016). Exposure of the invasive breast cancer cell line iMCF-7 to MoO_3 at 0.4 mg/mL concentration, induced apoptosis and generated reactive oxygen species (ROS) in these cells (Anh Tran et al. 2014). A similar effect was observed in G361 melanoma cells, where cell viability was reduced by more than 50% when exposed to 5 mg/mL of molybdenum oxide-polycaprolactone nanofiber. Probable mechanism was induction of mitochondria-dependent apoptosis (Janani et al. 2018). Conversely, no cytotoxic effect was observed when human macrophages were exposed to a 0.1 mg/mL concentration of MoO_3 2D nanoribbons (Gray et al. 2018).

Recently, we synthesized MoO_3 nanowires and nanotubes from $Mo_6S_2I_8$ nanowires via oxidation in air. Nanowire morphology of this starting material is preserved during oxidation, but the resulting MoO_3 nanowires are polycrystalline and porous. Scanning and transmission electron microscopy shows that these MoO_3 nanowires have grown into a semi-cylindrical shape with hollow or partially filled interior, depending on the diameter of the precursor nanowire (Varlec et al. 2016). These nanomaterials have unique shapes and degree of anisotropy and are patent protected (Mrzel et al. 2011) and one of their future applications could be contact nanocomposite coating aimed at using in public spaces. Therefore, assessing biocompatibility, i.e. functional responses of living cells exposed to these newly synthesized MoO_3 NPs, is needed.

Herein, we investigated the biological effect of MoO_3 NPs on human keratinocytes. We used HaCaT cells as a cell model of human skin which would be the first cells that come in contact with MoO_3 NPs containing polymer coating. To assess the biocompatibility of MoO_3 NPs, their effect on cytotoxicity, induction of apoptosis, DNA damage, production of ROS and changes in major cell-survival and inflammatory signaling-pathways was investigated. The short time exposure of up to 1 h, of HaCaT cells to MoO_3 NPs in an antimicrobial concentration of 1 mg/mL had no influence on cell survival nor did it induce changes in the amount of ROS or proteins involved in antioxidant defence. We detected no significant DNA damage or release of pro-inflammatory cytokines. Activation of the p38 and ERK MAP-kinase pathway was however noticed. Upon longer time exposure, namely 6 h and 24 h, we observed moderate release of the pro-inflammatory cytokine interleukin 6 (IL-6), increased DNA damage and increased percentage of caspase-independent apoptosis. Data presented here provide valuable information on the potential mechanisms involved in the MoO_3 NPs-induced cytotoxicity. Overall, this study allows us to conclude that short exposure of keratinocytes to MoO_3 NPs, especially for periods up to 1 h, has no significant impact on cell survival. However, exposing HaCaT cells to MoO_3 NPs did induce secretion of IL-6 and activated MAP kinases, therefore, further studies are needed in order to be able to propose that MoO_3 NPs pose no threat to human health.

2. Materials and methods

2.1. Preparation and characterization of MoO_3 NPs

The MoO_3 nanowires were synthesized from $Mo_6S_2I_8$ nanowires (Nanotul Ltd.) by oxidation at 285 °C for 24 h. The morphology of the nanowires was assessed using a SEM Supra 36 V P, Carl Zeiss. For SEM studies, the as-grown MoO_3 nanowires were put onto a carbon adhesive tape. For SEM analysis of MoO_3 nanowires dissolved in cell culture growth medium, Dulbecco Modified Eagle's Medium (DMEM; Sigma Aldrich, USA) or Eagle's Minimum Essential Medium (EMEM; Sigma Aldrich, USA) in a concentration of 1 mg/mL, were mixed for 6 h on a magnetic stirrer at 132 x g at room temperature (RT), left for 18 h, and then centrifuged at 661 x g for 3 min for separation from the growth medium. The residual was washed three times in isopropanol and drop casted directly onto a SEM aluminium holder. The pH values and conductivity were measured by Seven Excellence Multiparameter, (Mettler Toledo) with the probe InLab Expert Pro-ISM for pH and InLab 731-ISM probe for conductance measurements.

2.2. Cell culture

Spontaneously immortalized human keratinocyte HaCaT cells (Boukamp et al. 1988) were grown in DMEM supplemented with 10% of fetal bovine serum (FBS; Sigma Aldrich, USA; DMEM-FBS or exposed to MoO_3 NP in EMEM supplemented with 10% FBS (EMEM-FBS), and incubated at 37 °C with 5% CO_2 in a humidified atmosphere. Cells were regularly screened for mycoplasma presence with Hoechst 33258 staining.

2.3. Treatment design

MoO_3 powder was dissolved in EMEM, and the resulting solution was vigorously mixed by vortexing for at least two times, every 30 min, at RT. Solution was incubated at 4 °C overnight, and then filtered using a filter with 0.45 μm pores. Filtering did not affect the concentration of MoO_3 dissolved in EMEM, as determined by UV–vis absorption spectroscopy (data not shown). The filtered solution was further supplemented with 10% FBS and stock solutions with final concentrations of 2 mg/mL were prepared. Depending on the experimental set-up, cells were grown in DMEM-FBS and exposed to the appropriate concentration of MoO_3 dissolved in EMEM-FBS. Treatment lasted for 1 h, 6 h or 24 h, and cells were further cultured in DMEM-FBS. For each analysis, three biological replicates were performed.

2.4. Cell viability assay

To determine a possible cytotoxic effect of MoO_3 on human HaCaT cells, the MTT assay (Mosmann 1983) was performed. Cells were seeded in 96-well tissue culture plates (7×10^3 cells/well), and 24 h later, treated with MoO_3 (concentration range of 0.25–2 mg/mL). After treatment, medium was replaced with fresh DMEM-FBS and cells were grown for a further 72 h. Media was removed, and 1X MTT solution was added into each well and the plate incubated (37 °C, 5% CO_2) for 4 h, allowing formazan crystals to form. After 4 h, the resulting MTT-formazan products were dissolved using DMSO, and their absorbance measured using a microplate reader at 600 nm.

2.5. Quantitative polymerase chain reaction and ELISA assay

Expression of pro-inflammatory cytokines was assessed on gene expression levels by a quantitative polymerase chain reaction (qPCR) following reverse transcription of total RNA, which was isolated from cells. The amount of secreted cytokines on the other hand was measured by ELISA. Cells were seeded in 6-well tissue culture plates (5×10^5 cells/well), and 24 h later, treated with MoO_3 or a bacterial lipopolysaccharide (LPS) solution as positive control. After treatment, cells were collected and total RNA was isolated using a High Pure RNA Isolation kit (Roche, USA). Supernatants from the corresponding wells were used for ELISA. RNA was reverse-transcribed into first strand complementary DNA (cDNA) by a High-Capacity cDNA Reverse Transcription kit (Applied Biosystems, USA). cDNA was then analysed by qPCR on a StepOnePlusTM Real-Time PCR System (Thermo Fischer Scientific, USA) using the Sybr®Green reagent (Applied Biosystems, USA). PCR conditions were as follows: initial denaturation for 10 min at 95 °C, 40 cycles of 15 s at 95 °C and 1 min annealing at 60 °C. The StepOne Software (v 2.3) (Applied Biosystems, USA) was used to determine Ct values. The housekeeping gene GAPDH was used for assessing ΔΔCt, and fold changes were calculated using the standard $2^{-\Delta\Delta Ct}$ method (Livak and Schmittgen 2001). The PCR primers for analysed genes are listed in Table 1. Human IL-6 Uncoated Elisa, Human IL-8 Uncoated Elisa and Human IL-1 beta ELISA Ready-SET-Go!™ (Invitrogen, USA) were used according to the manufacturer's instructions. For IL-8

analysis, samples were diluted 5 times in growth medium.

2.6. Western blot

We used Western blot for analyse activation or amount of transcription factors and other proteins involved in cell survival, ROS pathway or immune response. Cells seeded in 6-well tissue culture plates (5×10^5 cells/well) were treated with MoO_3 solution or appropriate positive control (0.002% H_2O_2 solution), and after treatment, lysed with Laemmli buffer (heated to 95 °C), scraped off the plate, sonicated and boiled for 3 min. Proteins were separated using 10% SDS-PAGE and transferred to nitrocellulose membrane (Amersham Protran, GE Healthcare, USA). Membrane was blocked with 5% milk in Tris-Buffered Saline containing 1% Tween-20 and probed with the following primary antibodies: p-p38 (Santa Cruz Biotechnology, sc-166182); p38 (Santa Cruz Biotechnology, sc-535), pERK (Santa Cruz Biotechnology, sc-7383), ERK (Santa Cruz Biotechnology, sc-94), pJNK (Santa Cruz Biotechnology, sc-6254), JNK (Santa Cruz Biotechnology, sc-7345) Caspase-3 (Cell Signaling Technology, #9662), Caspase-8 (Cell Signaling Technology, #9746), Caspase-9 (Cell Signaling Technology, #9502), Sod2/MnSod (Abcam, #13533) and catalase (Abcam, #1877). Following incubation, blots were visualized with the appropriate horseradish peroxidase-conjugated IgG antibody. Detection was done with a Pierce™ ECL Western Blotting Substrate (Thermo Fischer Scientific, USA), while signals were detected using a ChemiDoc™ Imaging System (Bio-Rad, USA). Densitometry was performed with the ImageJ software (J52.A). Proteins were normalized to the total protein stained with amidoblack and the results were presented as relative expression or activation of proteins in treated samples compared to control samples.

2.7. Immunofluorescence

Activation of the NF-κB signalling pathway and induction of DNA damage following MoO_3 exposure were both determined by immunofluorescence. DNA damage was assessed via the amount of γ-H2AX foci, which is a hallmark of double DNA strand breaks (Bressy et al. 2017). HaCaT cells were seeded on coverslips in 24-well tissue culture plates (3×10^4 cells/well), which were incubated in FBS for 2 h (37 °C, 5% CO_2) prior seeding. 48 h later, cells were treated with MoO_3, or with LPS or H_2O_2 (0.002%). The latter two served as positive controls for determining NF-κB activation and induction of DNA damage, respectively. After treatment, cells were washed with PBS and incubated in cold 96% methanol for 10 min at −20 °C (NF-κB) or 2% paraformaldehyde in PBS for 12 min at RT and 0.5% Triton X-100/PBS for 10 min (γ-H2AX). After fixation and permeabilization, samples were washed with PBS, blocked with 3% bovine serum albumin in PBS for 30 min at RT and incubated with a primary antibody specific for pNF-κβ (Santa Cruz Biotechnology, sc-166748) or γ-H2AX (Abcam, ab11174) in 5% BSA in PBS for 1 h at RT. Samples were again washed with PBS and then incubated with the appropriate Alexa Fluor-conjugated secondary antibody in 5% BSA in PBS for 1 h, at RT and in the dark. Coverslips were mounted in mounting medium containing DAPI (Fluoromount G, Southern Biotech). Confocal microscopy analyses were performed using the Leica TCS SP8 X (Leica, Germany) with a 63x objective. Approximately 50 cells per glass were imaged throughout all sample slides. Images were processed with the Leica Application Suite X (LAS X, Leica, Germany) software platform. To measure activation of the NF-κB signalling pathway, the percentage of nuclei with pNF-κB signal was determined. For DNA damage analysis on the other hand, images were interpreted based on the number of γ-H2AX foci, where nuclei with more than 10 foci per nucleus were considered as positive.

Table 1
Primer sequences for qPCR analysis of IL-6, IL-8, IL-1β and TNF-α gene expression.

Gene ID	Primer sequences
IL-6	F: 5'CAATGAGGAGACTTGCCTGG3' R: 5'GCACAGCTCTGGCTTGTTCC3'
IL-8	F: 5'GTTTTTGAAGAGGGCTGAGAATTC3' R: 5'ATGAAGTGTTGAAGTAGATTTGCTTG3'
IL-1β	F: 5'TGGCAATGAGGATGACTTGTTC3' R: 5'CTGTAGTGGTGGTCGGAGATT3'
TNF-α	F: 5'AACCTCCTCTCTGCCATCAA3' R: 5'GGAAGACCCCTCCCAGATAG3'

2.8. Detecting apoptosis via AO/PI staining

To test whether MoO_3 induces apoptosis, Acridine Orange (AO)/Propidium Iodide (PI) assay was performed. HaCaT cells were seeded in 24-well tissue culture plates (1×10^4 cells/well) and the next day, treated with MoO_3 or 0.002% H_2O_2 (as positive control). After 24 h of treatment, cells were stained with AO (4 μg/mL) and PI (4 μg/mL) mixture for 10 min in an incubator (37 °C, 5% CO_2). Cells were then washed once with warm PBS to remove any unbound AO, and PBS was again added to all the wells. Cells were visualized by the FLoid™ Cell Imaging Station (Thermo Fischer Scientific, USA). An average of 3 images per sample has been made.

2.9. Detection of ROS

HaCaT cells were seeded in 12-well tissue culture plates ($2{,}5 \times 10^4$ cells/well). After 48 h, cells were treated with either MoO_3 solution or 0.002% H_2O_2 solution (as a positive control). After treatment, cells were washed with PBS, trypsinized, resuspended with cold PBS supplemented with 10% FBS (FBS-PBS) and centrifuged for 5 min (RT, 1100 g). Cell pellets were resuspended in 5 μM 2',7'–dichlorofluorescin diacetate (H2DCFDA, Sigma) which is oxidized to dichlorofluorescin (DCF) by ROS. Unstained cells were resuspended in PBS-FBS. Cells were then incubated for 30 min at 37 °C and 5% CO_2 and the signal was analysed by flow cytometry using FACSCalibur (BD Biosciences, USA).

2.10. Statistical analyses

All biological data were collected in triplicates and expressed as mean ± SD. Statistical analyses (one way ANOVA or Student t test) were performed in GraphPad. Differences were considered to be statistically significant when $p < 0.05$.

3. Results

3.1. Comparison of MoO_3 NPs dissolved in EMEM and DMEM

The MoO_3 nanowires used in this study are synthesized from $Mo_6S_2I_8$ nanowires. They keep the characteristic sea urchin shape of precursor agglomerates and grow in the orthorhombic crystal structure (JCPD 76-1003). A single MoO_3 nanowire is up to 200 nm in diameter and up to 3 μm in length (Fig. 1). The specific surface area of a MoO_3 nanowire is 12,06 ± 0.05 m^2/g (Gradišar Centa et al. 2020).

In order to test their biological effects, MoO_3 NPs were dissolved in two commonly used cell culture media, EMEM and DMEM. DMEM contains up to four times more vitamins and amino acids, and two to four times more glucose than EMEM. HaCaT cells can however be equally grown in both media. We exposed MoO_3 nanowires for 24 h to either EMEM or DMEM and observed their morphology by SEM. In DMEM, dissolving of MoO_3 nanowires was less pronounced and the sea urchin morphology was preserved, while in EMEM, the nanowires dissolved better, and the sea urchin morphology fell apart to individual nanowires (Fig. 2, A). The MoO_3 NPs surfaces were porous, especially when dissolved in EMEM. The observed increased porosity could rather be attributed to washing in isopropanol, which always contains residuals of water, than exposure to growth medium, or an inadequate dissolving in the growth medium.

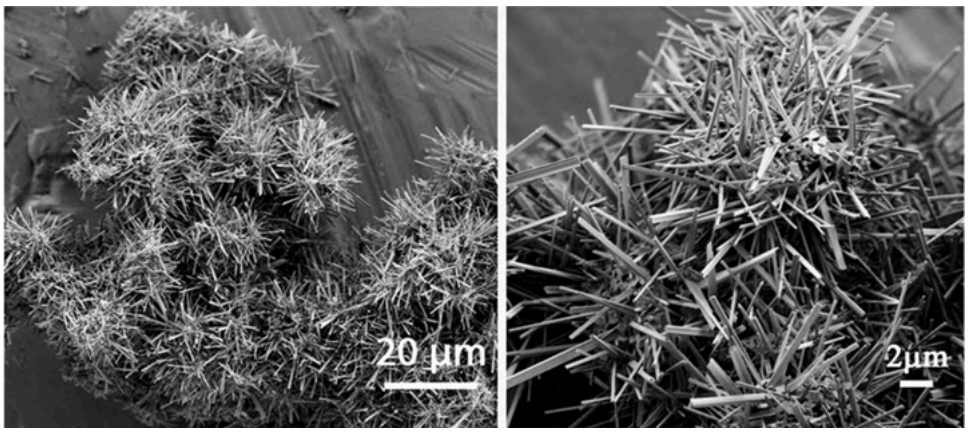

Fig. 1. Scanning electron microscopy images of MoO_3 nanowires, self-assembled in a sea urchin growth morphology.

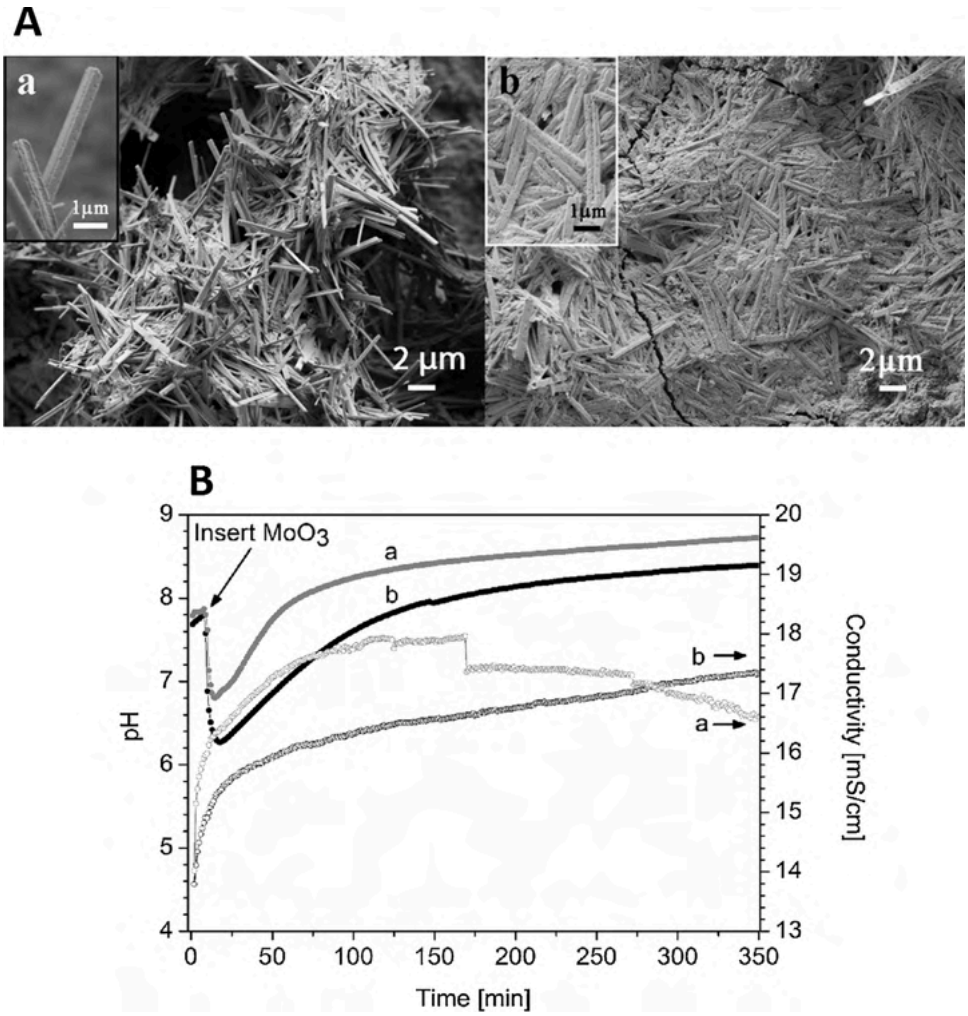

Fig. 2. Characterization of MoO_3 nanowires dissolving in cell growth medium. Scanning electron microscopy images of MoO_3 nanowires after dissolving in DMEM (a) or EMEM (b) (A). The inserts show porous surfaces of the nanowires in both cases. Time evolution of conductivity and pH values during dissolution of MoO_3 nanowires in DMEM (a) or EMEM (b) (B).

Dissolving MoO_3 nanowires in growth medium caused an initial drop in pH value in 15 min; from 8.3 to 6.8 in DMEM, and in 18 min; from 7.8 to 6.3 in EMEM. The pH values however, start to increase, and in approximately 110 min, reached the starting values before MoO_3 NPs insertion. The pH values increase even further all the way to the end of the dissolving test (350 min), where the pH values were: 8.4 (EMEM) and 8.7 (DMEM) (Fig. 2, B). From the steeper slope of the DMEM curve, it is possible to conclude lower concentration of dissolved MoO_3, which is in accordance with SEM observations.

The observation that growth medium can influence MoO_3 NPs solubility was further supported by the data obtained in our conductivity measurement. Showed in Fig. 2, B, during dissolving of MoO_3 in DMEM,

conductivity increased at first, then reached a saturation plateau, before starting to decrease. A sudden drop in conductivity 160 min after MoO_3 insertion could be explained with an artefact measurement in dynamic vicinity of the electrode. Decrease in conductivity with time implies reduction in the number of ions (H_3O^+, MoO_4^{2-}) due to their neutralization by components in DMEM. Unlike DMEM, the conductivity in EMEM steadily increased from the time of MoO_3 insertion until the end of the experiment. Thus, MoO_3 NPs were dissolved in EMEM for all subsequent experiments.

3.2. Short time exposure to MoO_3 NPs in concentration of 1 mg/mL had no influence on HaCaT cells survival

In order to study the cytotoxic effect of MoO_3 NPs, the MTT assay was performed following exposure of HaCaT cells to different concentrations of MoO_3 NPs (0.25 mg/mL-2 mg/mL). These concentrations were chosen based on their antimicrobial properties obtained in our previous research (Gradišar Centa U. et al. unpublished data) with these compounds. As shown in the Fig. 3, exposing HaCaT cells to MoO_3 NPs for 1 h had no significant influence on cell survival in any of the studied concentrations. However, after 6 h of exposure, a toxic effect was observed with the 2 mg/mL MoO_3 NPs concentration. At this time point and concentration, 20% of the cells died, and after 24 h, none of the cells survived. Lower concentrations showed a similar trend, but the toxicity was conversely much lower even after longer periods of exposure. Compared to controls, treatment of cells with 1.5 mg/mL MoO_3 NPs for 6 h and 24 h resulted in cell deaths of 8% and 62%, respectively, while treatment with 1 mg/mL for the same time periods resulted in a cell death of 2% and 55%, respectively. Concentrations lower than 1 mg/mL had no significant influence on cell survival.

Since MoO_3 NPs at 1 mg/mL concentration still exhibited antimicrobial properties (Gradišar Centa U. et al. unpublished data) but showed no significant toxic effects on HaCaT cells survival during the short time exposure (up to 6 h), we decided to use this concentration in order to further investigate the biological effects of MoO_3 NPs.

3.3. MoO_3 NPs trigger the increase of pro-inflammatory cytokine IL-6 gene expression and protein secretion

It is known that nanoparticles can communicate with various biological components of the immune system (Liu et al. 2017), thus, we assessed gene expression of pro-inflammatory cytokines not only on transcriptional levels, but also on the level of cytokine secretion in HaCaT cells exposed to MoO_3 NPs. Long-term exposure, namely 24 h, to 1 mg/mL of MoO_3, profoundly increased expression of the pro-inflammatory cytokines IL-6, IL-8, IL-1β and TNF-α. Short term exposure on the other hand, influenced only IL-6 gene expression, which was 2 fold higher compared to control samples, while after 24 h, expression of the IL-6 gene was 25 fold higher in cells exposed to MoO_3 NPs (Fig. 4A) compared to control treated cells. Exposing HaCaT cells to MoO_3 NPs caused elevated secretion of IL-6 after 6 h and 24 h, 2.5 and 2.2 fold respectively, compared to the control. One hour of exposure did not cause any significant change in secreted amount of IL-6. Exposing HaCaT cells to 1 mg/mL of MoO_3 NPs did not induce secretion of IL-8 and IL-1β in any observed time point (Fig. 4B).

3.4. Exposure to MoO_3 NPs induced activation of p38 and ERK mitogen-activated protein kinases

Mitogen-activated protein kinase (MAPK) signalling cascades are known to regulate cellular responses to external stresses as well as expression of multiple genes that regulate the inflammatory response and cytokine production (Arthur and Ley 2013). As shown in Fig. 5A, we observed increased phosphorylation of p38 and ERK, but not of JNK, when HaCaT cells were exposed to 1 mg/mL of MoO_3 NPs. Phosphorylation of p38 was the strongest 1 h after the exposure, and even though phosphorylation decreased over time, it was still increased 24 h after exposure. Relative activation of p38, expressed as a ratio of p-p38/p38 in the MoO_3 NPs exposed cells, compared to control cells, was 4.4, 3.2 and 2.7 fold higher after 1 h, 6 h and 24 h, respectively. On the contrary, ERK phosphorylation was time dependent, i.e. it increased with longer exposure times. Relative activation of ERK expressed as a ratio of

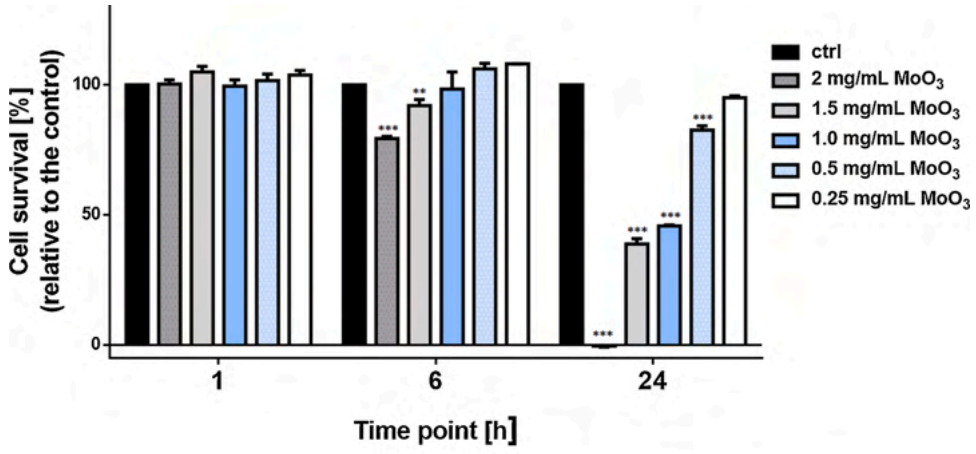

Average survival (%)	1h	6h	24h
ctrl	100	100	100
0.25 mg/mL MoO_3	103.7706699	108.0373668	95.01117503
0.5 mg/mL MoO_3	101.6190655	106.1035724	82.56484862
1.0 mg/mL MoO_3	99.49333876	98.32539409	45.71288424
1.5 mg/mL MoO_3	104.9195862	92.00274998	38.74762466
2.0 mg/mL MoO_3	100.2541417	79.3698985	-0.467085172

Fig. 3. Cell survival of HaCaT cells exposed for 1 h, 6 h and 24 h to different concentrations of MoO_3 NPs. Data are presented as mean ± SD made in four replicates, relative to the control samples. Representative data of three independent experiments which yielded similar results are shown. *, $P < 0.05$; **, $P < 0.01$; ***, $P < 0.001$.

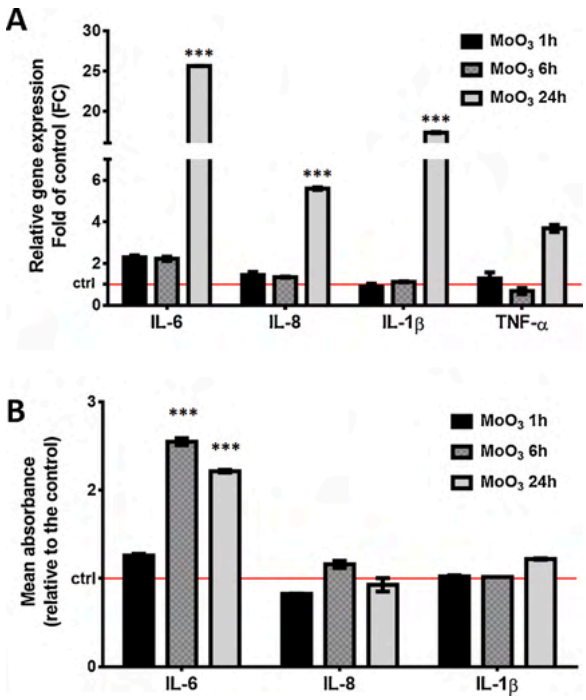

Fig. 4. Gene expression (A) and release of pro-inflamatory cytokines (B) in HaCaT cells exposed to 1 mg/mL MoO_3 NPs for 1 h, 6 h and 24 h. Relative gene expression is presented as a fold change relative to control samples. Analysis of cytokine release was performed by ELISA. Secretion of cytokines is presented as relative to the control samples. Representative data of two independent experiments which yielded similar results are shown. *, $P < 0.05$; **, $P < 0.01$; ***, $P < 0.001$.

pERK/ERK in MoO_3 NPs exposed cells compared to control cells, was 2.1, 3.3 and 2.9 fold higher after 1 h, 6 h and 24 h, respectively.

Once p38 is phosphorylated, the NF-κB transcription factor gets activated (Sakai et al. 2002), which in turn leads to gene expression of cytokines and other inflammatory molecules (Lawrence 2009). In order to determine whether exposure to MoO_3 NPs is capable of inducing the activation of NF-κB, the amount of cells which demonstrate nuclear localization of the p65 subunit of NF-κB was determined by immunofluorescence. Unexpectedly, compared to non-treated cells, we detected decreased activation of NF-κB in all time points following exposure of HaCat cells to MoO_3 NPs (Fig. 5B).

3.5. Short time exposure of human keratinocytes to MoO_3 NPs did not induce DNA damage or ROS production

Exposing human cells to metal nanoparticles may result in an increased production of ROS and subsequently DNA damage (Wan et al. 2012). We therefore, assessed both the generation of ROS and induction of DNA damage after exposing HaCaT cells to MoO_3 NPs. As shown in Fig. 6, only long-term exposure to MoO_3 NPs significantly induced DNA double strand breaks, evidenced as phosphorylation of histone H2 (γ-H2AX) in HaCaT cells. Compared to control cells, 7.5 fold more cells exposed to MoO_3 NPs for 24 h were positive for the γ-H2AX foci. At shorter exposure, up to 1 h, DNA damage was not detected, while 6 h of exposure induced a 2.8 fold more of cells positive for the γ-H2AX foci, when compared to the control samples.

Interestingly, exposure to MoO_3 NPs induced production of intracellular ROS only after 24 h. This increase was moderate but distinctive. No significant change in ROS level was detected between control cells and cells exposed to MoO_3 NPs for 1 h or 6 h (Fig. 7A). Increase in ROS production following 24 h of exposure to MoO_3 NPs could be attributed to the decreased level of superoxide dismutase 2 (SOD2), which is one of the primary mitochondrial antioxidants (Fig. 7B). Contrary to SOD2 amount, expression of catalase was slightly increased following exposure to MoO_3 NPs (6 h and 24 h). These data imply that long term exposure to 1 mg/mL MoO_3 NP might alter the antioxidant system in human keratinocytes.

3.6. Increased percentage of apoptotic cells after long time exposure to MoO_3 NP is caspase independent

Since a decreased survival of HaCaT cells at longer exposure to MoO_3 NPs was observed, the mechanisms of cell death were investigated. The AO/PI staining, which allows differentiation between live and apoptotic/necrotic cells, was performed. Cells exposed to MoO_3 NPs for 1 h exhibited meagre cell death (3.7% cells in apoptosis). When the cells were exposed to MoO_3 NPs for 6 h or 24 h, an increased but yet minimal cell death (13.5% and 20.1% of apoptotic cells, respectively) was again observed (Fig. 8A).

To assess the mechanism behind the observed increase in apoptosis, activation of caspases, proteins playing an essential role in programmed cell death, was studied in HaCaT cells exposed to MoO_3 NPs. Only procaspase-3 and procaspase-8, without their cleaved products (i.e. active forms), were detected (Fig. 8B). We did detect cleaved caspase-9 but only after a longer exposure (24 h) to MoO_3 NPs. When cells were exposed to MoO_3 NPs for 1 h and 6 h, the same amount as in the control cells, of cleaved caspase-9 was detected. Longer exposure to MoO_3 NPs, i.e. 24 h, decreased amount of cleaved caspase-9. Hence, the analysis of procaspase-3, -8 and -9 revealed that MoO_3 NPs exposure did not induce activation of caspase-3, also known as executioner caspase, but only the initiator caspase, caspase-9. Since caspase-3 activation induces the apoptosis process, we can conclude that the observed cell death 6 h or 24 h after exposure to MoO_3 NPs is caspase-independent.

4. Discussion

An innovative approach to preventing the dissemination of microorganisms in healthcare units and public environments by applying transition metal oxides as antimicrobial agents in surface coatings has recently been proposed. One of the promising candidates for manufacturing this type of coatings is MoO_3 (Zollfrank et al. 2012). Recently, synthesis of MoO_3 nanowires and nanotubes via transformation of molybdenum-sulfur-iodine nanowires was reported. This unique synthesis route results in an interesting morphology, comprises porous nanowires and nanotubes (Varlec et al. 2016), hence, could be considered for possible future applications, such as antimicrobial surface coatings. The potential human health risks following exposure to MoO_3 NPs is a very important issue and needs to be assessed prior their potential application.

Here, we investigated the biological effects of MoO_3 NPs on human keratinocytes. HaCaT cells were used as a cell model for human skin due to the assumption that any future application of MoO_3 NPs will be in surface coatings, and as such, they could come in contact with the human skin. HaCaT cell line is a non-tumorigenic monoclonal cell line, adapted to long term growth without feed-layer or supplemented growth factors. It exhibits normal morphogenesis and expresses all the major surface markers and functional activities of isolated keratinocytes, and as such is appropriate model for studying human skin (Colombo et al. 2017).

In order to be exposed to the cells, the MoO_3 NPs were dissolved in two commonly used media for growing HaCaT cells, DMEM and EMEM. MoO_3 NPs dissolved in DMEM did not create a stable dissolution and had a steeper slope of the pH curve; indicating a lower concentration of dissolved MoO_3, which is in accordance with SEM observations. Since conductivity is directly linked to the total amount of solids dissolved (Rusydi 2018), a strong decrease in conductivity was able to further corroborate the lower solubility of MoO_3 NPs in DMEM. When dissolved in DMEM, MoO_3 NPs also became very toxic for the cells (data not

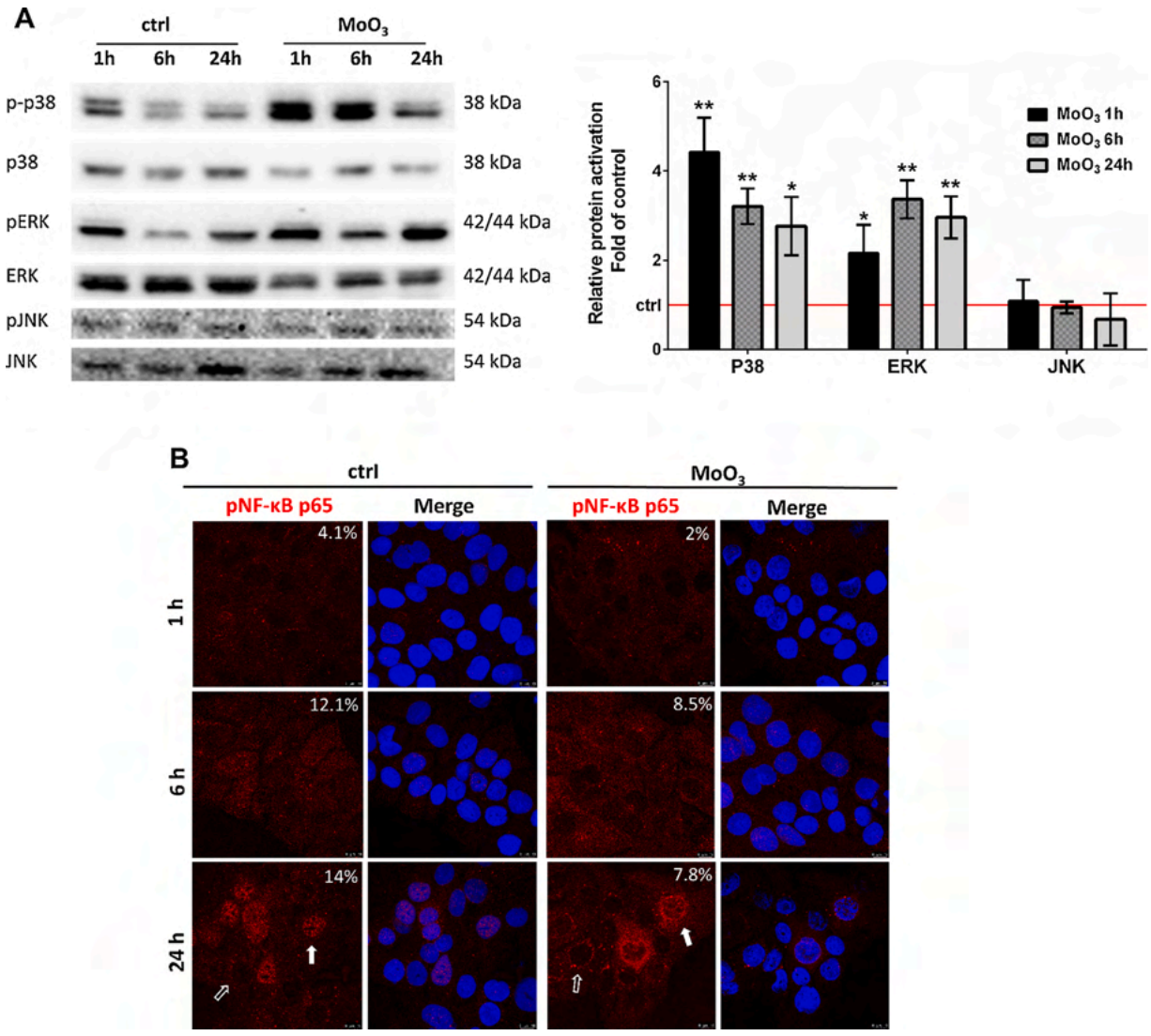

Fig. 5. Activation of mitogen activated protein kinases and NFκB in HaCaT cells exposed to 1 mg/mL MoO_3 NPs for 1 h, 6 h and 24 h. Phosphorylation of p38, ERK, and JNK in HaCaT cells treated with MoO_3 (A). Densitometry analysis is shown on the right hand side. Data are expressed as means ± SD from three independent experiments, and are presented as fold increase over control in phosphorylated protein levels normalized to total protein levels. Amidoblack staining was used as a control for gel loading. *, $P < 0.05$; **, $P < 0.01$; ***, $P < 0.001$. NF-κB nuclear translocation in control and HaCaT cells treated with MoO_3, and observed by confocal microscopy (B). Full arrows indicate positive nuclear signal for pNF-κB p65, while empty arrows indicate cells without nuclear pNF-κB p65 signal. The percentage of cells with a positive nuclear signal for pNF-κB p65 is shown in the upper right corner of each panel. A representative data of two independent experiments which yielded similar results is shown.

shown), however further investigation of the observed effect is out of scope of this study. Hence, for all subsequent evaluations of the biological effects of MoO_3 in this study, MoO_3 NPs were dissolved in EMEM.

The impact of MoO_3 NPs cytotoxicity on HaCaT cells, which was evaluated by the MTT assay showed that a concentration of 1 mg/mL had no distinctive influence on HaCaT cell survival at shorter time exposures. So far there is only one report regarding MoO_3 NPs toxicity in HaCaT cells. The IC_{50} values of MoO_3, prepared with a wet chemical method using ammonium molybdate as a starting precursor, for HaCaT cells was found to be around 400 mg/mL (Indrakumar and Korrapati 2019), which is approximately 200 fold higher than in our study. MoO_3 nanoparticles were considered mildly toxic in immortalized rat liver cells; as concentrations higher than 0.1 mg/mL caused a decrease in cell viability (Hussain et al. 2005). However, the same concentration of MoO_3 nanoparticles had no significant influence on spermatogonial stem cell growth; even at very low concentrations, 0.005-0.1 mg/mL (Braydich-Stolle et al. 2005). MoO_3 also proved to be toxic on cancer cells in lower concentrations spanning from 0.05 to 0.4 mg/mL (Anh Tran et al. 2014; Sivan et al. 2019). The discrepancy observed between different reports may be explained by differences in experimental environment, namely, the cell lines employed. Observed also indicates that MoO_3 NPs cytotoxicity highly depend on the synthesis procedure along with the physical properties of MoO_3 NPs. Regarding a possible cell death mechanism, our data suggests that the increased percentage of apoptotic cells observed after long time exposure to MoO_3 NPs is caspase-independent; which is contrary to what was reported in invasive human breast cancer iMCF-7 cells exposed to MoO_3 (Anh Tran et al. 2014).

Our study revealed that exposing HaCaT cells to MoO_3 NPs for 24 h increases the gene expression of pro-inflammatory cytokines IL-6, IL-8, IL-1β and TNF-α. In terms of MoO_3 NPs-induced cytokine secretion however, only IL-6 was increased when HaCat cells were exposed to the same concentration of MoO_3 NPs for 24 h. To the best of our knowledge there is only one report regarding chemokine expression after exposing cells to MoO_3 reporting no change in expression of IL-8 in human lung carcinoma cells A549 after exposing them to MoO_3, which is in line with

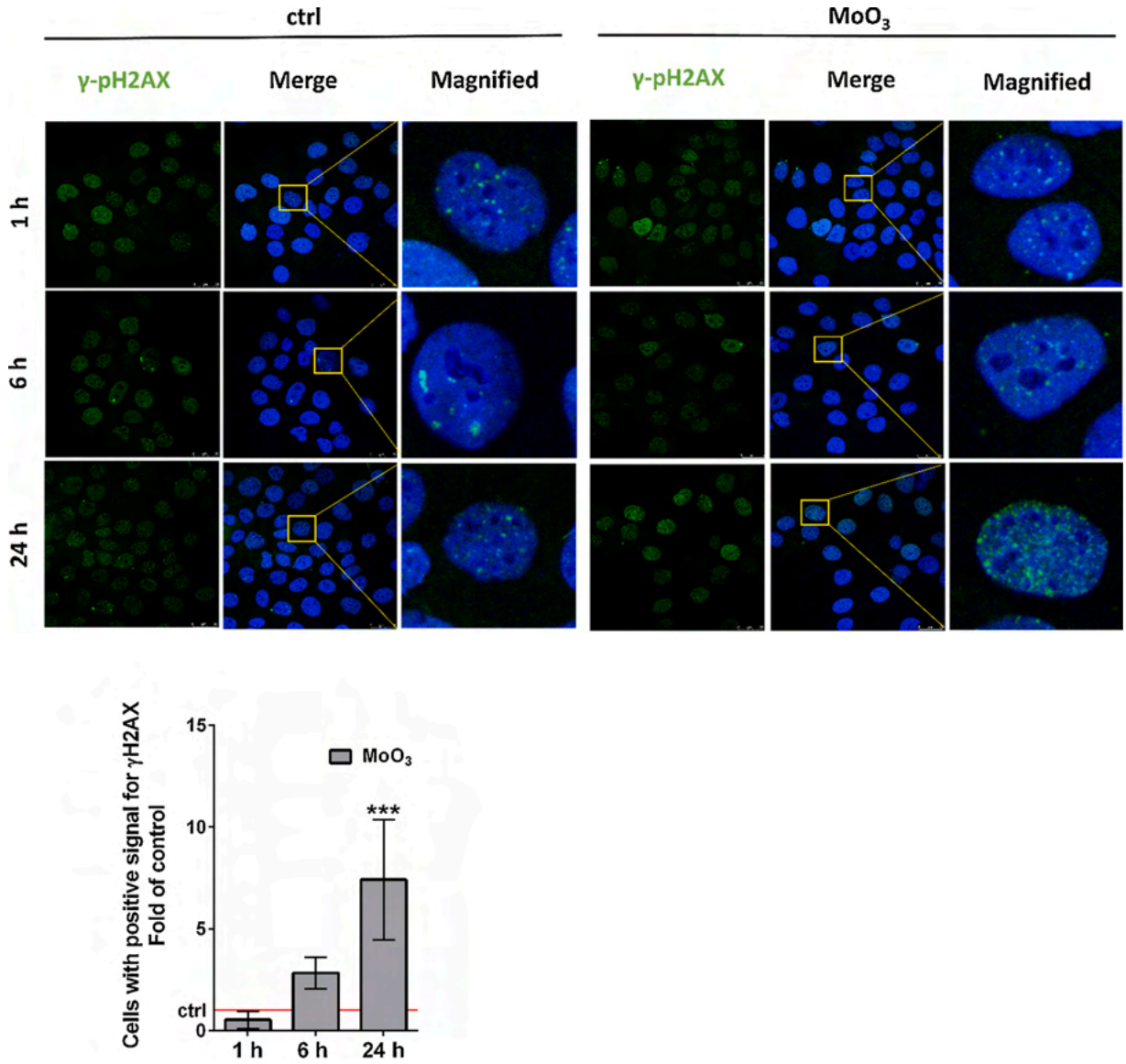

Fig. 6. DNA damage in HaCaT cells exposed to 1 mg/mL MoO_3 NPs for 1 h, 6 h and 24 h. Double strand DNA breaks evidenced as γ-H2AX staining (green) visualized by confocal microscopy. Cell nuclei are stained by DAPI (blue). The ratio between the percentage of nuclei positive for γ-H2AX staining in cells exposed to MoO_3 NPs, to that of the control cells, is presented in the lower panel. *, $P < 0.05$; **, $P < 0.01$; ***, $P < 0.001$. A representative data of two independent experiments which yielded similar results is shown. (For interpretation of the references to color in this figure legend, the reader is referred to the web version of this article.)

our data (Horie et al. 2018). Other cytokines that we have analysed here, until now, have not been assessed. IL-6 is characterized as a pleiotropic cytokine and has context-dependent pro- and anti-inflammatory properties (Hunter and Jones 2015). Since it is required for normal wound repair, IL-6 is produced by normal human keratinocyte and may be associated rather with modulation of keratinocyte differentiation than proliferation (Sugawara et al. 2001). Hence, one could speculate that increased secretion of IL-6 following exposure to MoO_3 NPs should not be considered as a potential risk to human health. Additionally, it should be stressed out that increased secretion of IL-6 was observed after longer exposure, i.e. after 6 h and 24 h, and not after 1 h. We assume the latter to be the optimal time frame in which potential MoO_3 containing coatings would be in contact with the skin.

It is known that nanoparticles can activate MAP kinases (Marano et al. 2011), which in turn can influence expression of genes that are involved in cell survival, inflammatory response and cytokine production (Arthur and Ley 2013). We found, that exposure to MoO_3 NPs induced phosphorylation, and hence, activation of ERK and p38, but not JNK. Since both p38 and ERK converge towards NF-κB we also determined activation status of this transcription factor. In HaCaT cells exposed to MoO_3 NPs, we observed decreased activation of NF-κB. A similar outcome was reported for zinc oxide nanoparticles (Kim and Jeong 2015). Even though all three signalling molecules, p38, ERK and NF-κB can be involved in the induction of IL-6 gene expression and secretion (Craig et al. 2000; Perez et al. 2009), we assume that the increased IL-6 secretion observed in our study is p38/ERK- and not NF-κB-mediated. To the best of our knowledge, this study is the first to demonstrate MoO_3 NPs-induced activation of MAPKs.

Oxidative stress is one of the most important mechanisms governing nanomaterial-mediated toxicity (Fu et al. 2014). To the best of our knowledge there are only few studies regarding MoO_3 nanoparticles and ROS production, including our research. We detected increased ROS production in HaCaT cells only after 24 h exposure to MoO_3 NPs, which is in agreement with what was observed in not only invasive human breast cancer iMCF-7 cells following exposure to MoO_3 nanoplates (Anh Tran et al. 2014), but also in the human squamous carcinoma A431 cells treated with MoO_3 (Indrakumar and Korrapati 2019). The authors did not reflect on possible mechanism. A possible reason for the increase in

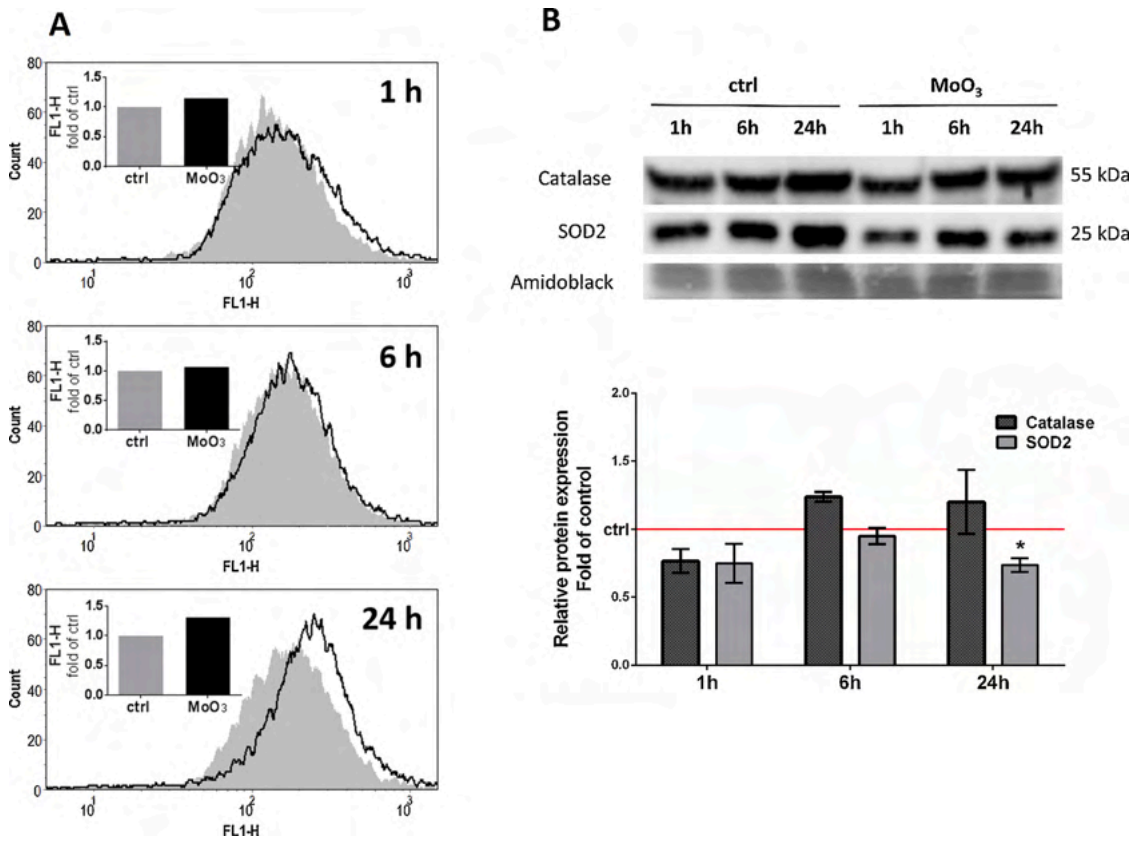

Fig. 7. The amount of ROS (A) and antioxidant proteins (B) in HaCaT cells exposed to 1 mg/mL MoO_3 NPs for 1 h, 6 h and 24 h. Levels of ROS were measured by measuring the fluorescence intensity of DCF in each treated sample by flow cytometry. Black line represents cells exposed to MoO_3 NPs, grey shaded histogram represents control cells. A representative data of two independent experiments which yielded similar results is shown. SOD2 and catalase protein levels in control and HaCaT cells treated with MoO_3 were analysed by Western blot. Densitometric analysis is shown in the lower panel. Data are expressed as means ± SD from two independent experiments, and are presented as fold increase over control samples normalized to total protein levels. Amidoblack staining was used as control for gel loading. *, $P < 0.05$; **, $P < 0.01$; ***, $P < 0.001$.

ROS production following MoO_3 treatment observed in our research could be decreased SOD2 levels; as SOD2 is one of the primary mitochondrial antioxidants (Fukai and Ushio-Fukai 2011). There are several transcriptional factors, including NF-κB, FOXO3a, SIRT, AP-2 and Sp1, that have been shown to play important roles in regulating the constitutive or inductive expression levels of SOD2 (Kim et al. 2017; Miao and St Clair 2009). We assume that the decreased expression of SOD2 observed in our study could be due to the decreased activation of NF-κB that we saw in HaCaT cells after exposing them to MoO_3 NPs. Decreased SOD2 level was reported also for osteoblast cells exposed to titanium dioxide nanoparticles. Authors attributed this to decreased SIR3 protein level (Niska et al. 2015). Current literature suggests that the nanowire internalization is taking place through both phagocytosis and micropinocytosis (Abariute et al. 2019; Safi et al. 2011; Zimmerman et al. 2016). Depending on their size nanowires can localize to lysosomes where they can puncture the enclosing membrane and cause lysosomal damage (Ji et al. 2012; Lehmann et al. 2019) leading to ROS production as well as cell death. It has been shown that MoO_3 nanoribbons internalized by macrophages are localized within lysosomes but do not disrupt lysosomal membrane integrity (Gray et al. 2018). Studying MoO_3 NPs cell localization was beyond our study. Data obtained in our study suggests that long term exposure to 1 mg/mL MoO_3 NPs might alter the antioxidant system in human keratinocytes. The increased ROS production observed in these HaCaT cells after 24 h exposure to MoO_3 NPs could be the cause of DNA damage induction. Increased DNA damage was also reported in invasive human breast cancer iMCF-7 cells exposed to MoO_3 (Anh Tran et al. 2014).

The secretion of IL-6, increased DNA damage and ROS production in HaCaT cells after long-term exposure to MoO_3 NPs indicates that these NPs can promote oxidative-inflammatory effects in human keratinocytes, and therefore, suggests that long-term exposure to MoO_3 NPs could induce production of pro-inflammatory mediators on human skin. In order to reveal the exact mechanism of how MoO_3 NPs affects HaCaT cells under long term exposure, further study is necessary.

5. Conclusion

Exposing HaCaT cells to MoO_3 NPs at a concentration of 1 mg/mL during short periods, namely up to 6 h, had no significant effect on cell survival, ROS production or the expression of proteins involved in antioxidant defence. Although DNA damage was not significantly induced, the activation of ERK and p38 MAP kinases, along with a moderate release of the pro-inflammatory cytokine IL-6 and increased level of caspase-independent apoptosis were observed. Overall, our data indicate that exposing keratinocytes to 1 mg/mL MoO_3 NPs antimicrobial water-based solution in durations that are less than 1 h, exhibits no significant cytotoxicity. The MoO_3 NPs do however trigger cell signalling cascades that are involved in cell proliferation and inflammation, which should be taken into consideration when evaluating possible medical usage of MoO_3 NPs.

Declaration of Competing Interest

The authors reported no declarations of interest.

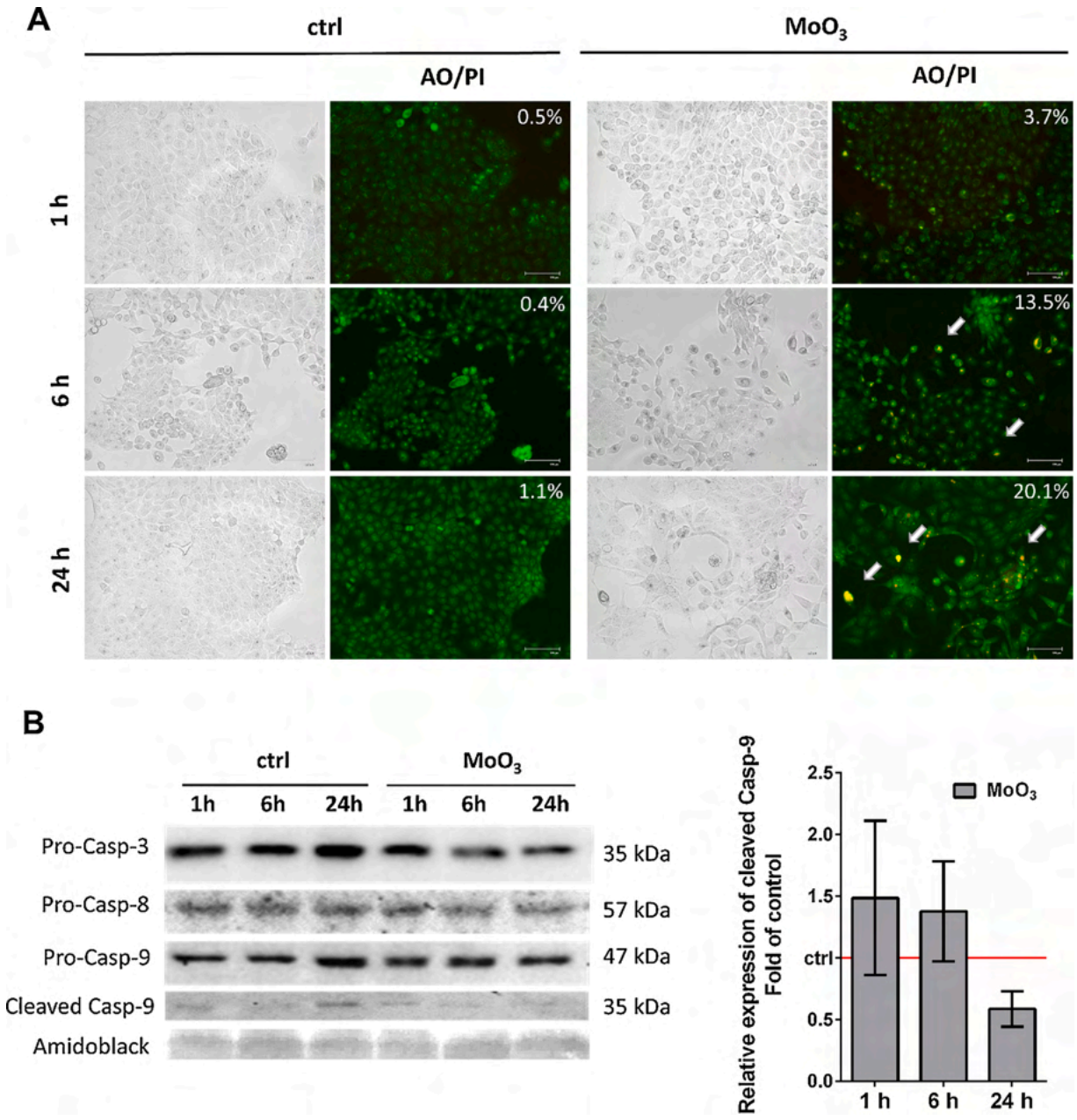

Fig. 8. Apoptosis in HaCaT cells exposed to 1 mg/mL MoO_3 NPs for 1 h, 6 h and 24 h. AO/PI staining of HaCaT cells after MoO_3 treatment (A). Cells showing apoptotic characteristics (green granulated AO and bright red PI in nuclei) are presented here as orange. White arrows are indicating apoptotic cells. Percentage of the AO/PI-positively stained, i.e. apoptotic cells, to the total cells is shown in the upper right corner of each panel. A representative data of two independent experiments which yielded similar results is shown. Western blot analysis of Caspase-3, Caspase-8 and Caspase-9 in HaCaT cells treated with MoO_3 (B). Densitometric analysis of cleaved Caspase-9 is shown on the right hand side. Data are expressed as means ± SD from two independent experiments, and are presented as fold increase over control samples normalized to total protein levels. Amidoblack staining was used as a control for gel loading. (For interpretation of the references to color in this figure legend, the reader is referred to the web version of this article.)

Acknowledgments

This work was financially supported by the Slovenian Research Agency through contracts P0-5544 and P1-0099, and by the Slovenia-Croatia bilateral project BI-HR/18-19-019. The authors would like to thank Ms Marina Šutalo for her technical assistance.

References

Abariute, L., Lard, M., Hebisch, E., Prinz, C.N., 2019. Uptake of nanowires by human lung adenocarcinoma cells. PLoS One 14, e0218122.

Anh Tran, T., Krishnamoorthy, K., Song, Y.W., Cho, S.K., Kim, S.J., 2014. Toxicity of nano molybdenum trioxide toward invasive breast cancer cells. ACS Appl. Mater. Interfaces 6, 2980–2986.

Arthur, J.S., Ley, S.C., 2013. Mitogen-activated protein kinases in innate immunity. Nat. Rev. Immunol. 13, 679–692.

Boukamp, P., Petrussevska, R.T., Breitkreutz, D., Hornung, J., Markham, A., Fusenig, N. E., 1988. Normal keratinization in a spontaneously immortalized aneuploid human keratinocyte cell line. J. Cell Biol. 106, 761–771.

Braydich-Stolle, L., Hussain, S., Schlager, J.J., Hofmann, M.C., 2005. In vitro cytotoxicity of nanoparticles in mammalian germline stem cells. Toxicol. Sci. 88, 412–419.

Bressy, C., Majhen, D., Raddi, N., Jdey, W., Cornilleau, G., Zig, L., Guirouilh-Barbat, J., Lopez, B.S., Bawa, O., Opolon, P., Grellier, E., Benihoud, K., 2017. Combined therapy of colon carcinomas with an oncolytic adenovirus and valproic acid. Oncotarget 8, 97344–97360.

Colombo, I., Sangiovanni, E., Maggio, R., Mattozzi, C., Zava, S., Corbett, Y., Fumagalli, M., Carlino, C., Corsetto, P.A., Scaccabarozzi, D., Calvieri, S.,

Gismondi, A., Taramelli, D., Dell'Agli, M., 2017. HaCaT cells as a reliable in vitro differentiation model to dissect the inflammatory/repair response of human keratinocytes. Mediat. Inflamm.
Craig, R., Larkin, A., Mingo, A.M., Thuerauf, D.J., Andrews, C., McDonough, P.M., Glembotski, C.C., 2000. p38 MAPK and NF-kappa B collaborate to induce interleukin-6 gene expression and release. Evidence for a cytoprotective autocrine signaling pathway in a cardiac myocyte model system. J. Biol. Chem. 275, 23814–23824.
Dastjerdi, R., Montazer, M., 2010. A review on the application of inorganic nano-structured materials in the modification of textiles: focus on anti-microbial properties. Colloids Surf. B 79, 5–18.
Fakhri, A., Nejad, P.A., 2016. Antimicrobial, antioxidant and cytotoxic effect of Molybdenum trioxide nanoparticles and application of this for degradation of ketamine under different light illumination. J. Photochem. Photobiol. B 159, 211–217.
Fu, P.P., Xia, Q., Hwang, H.M., Ray, P.C., Yu, H., 2014. Mechanisms of nanotoxicity: generation of reactive oxygen species. J. Food Drug Anal. 22, 64–75.
Fukai, T., Ushio-Fukai, M., 2011. Superoxide dismutases: role in redox signaling, vascular function, and diseases. Antioxid. Redox Signal. 15, 1583–1606.
Gold, K., Slay, B., Knackstedt, M., Gaharwar, A.K., 2018. Antimicrobial activity of metal and metal-oxide based nanoparticles. Adv. Ther. 1, 1700033.
Gradišar Centa, U., Kocbek, P., Belcarz, A., Škapin, S.D., Remškar, M., 2020. Polymer blend containing MoO_3 nanowires with antibacterial activity against Staphylococcus epidermidis ATCC 12228. J. Nanomater. 2020, 9754024.
Gray, E.P., Browning, C.L., Wang, M.J., Gion, K.D., Chao, E.Y., Koski, K.J., Kane, A.B., Hurt, R.H., 2018. Biodissolution and cellular response to MoO3 nanoribbons and a new framework for early hazard screening for 2D materials. Environ. Sci.-Nanotechnol. 5, 2545–2559.
Hajipour, M.J., Fromm, K.M., Ashkarran, A.A., de Aberasturi, D.J., de Larramendi, I.R., Rojo, T., Serpooshan, V., Parak, W.J., Mahmoudi, M., 2012. Antibacterial properties of nanoparticles. Trends Biotechnol. 30, 499–511.
Hasan, A., Morshed, M., Memic, A., Hassan, S., Webster, T.J., Marei, H.E., 2018. Nanoparticles in tissue engineering: applications, challenges and prospects. Int. J. Nanomed. 13, 5637–5655.
Horie, M., Shimizu, K., Tabei, Y., 2018. Validation of metallothionein, interleukin-8, and heme oxygenase-1 as markers for the evaluation of cytotoxicity caused by metal oxide nanoparticles. Toxicol. Mech. Method 28, 630–638.
Hunter, C.A., Jones, S.A., 2015. IL-6 as a keystone cytokine in health and disease. Nat. Immunol. 16, 448–457.
Hussain, S.M., Hess, K.L., Gearhart, J.M., Geiss, K.T., Schlager, J.J., 2005. In vitro toxicity of nanoparticles in BRL 3A rat liver cells. Toxicol. in Vitro 19, 975–983.
Indrakumar, J., Korrapati, P.S., 2019. Steering Efficacy of Nano Molybdenum Towards Cancer: Mechanism of Action. Biological Trace Element Research.
Janani, I., Lakra, R., Kiran, M.S., Korrapati, P.S., 2018. Selectivity and sensitivity of molybdenum oxide-polycaprolactone nanofiber composites on skin cancer: Preliminary in-vitro and in-vivo implications. J. Trace Elem. Med. Biol. 49, 60–71.
Ji, Z., Wang, X., Zhang, H., Lin, S., Meng, H., Sun, B., George, S., Xia, T., Nel, A.E., Zink, J.I., 2012. Designed synthesis of CeO_2 nanorods and nanowires for studying toxicological effects of high aspect ratio nanomaterials. ACS Nano 6, 5366–5380.
Karim, N., Afroj, S., Tan, S., Novoselov, K.S., Yeates, S.G., 2019. All Inkjet-printed graphene-silver composite ink on textiles for highly conductive wearable electronics applications. Sci. Rep.-Uk 9, 8035.
Kim, M.H., Jeong, H.J., 2015. Zinc oxide nanoparticles suppress LPS-induced NF-kappaB activation by inducing A20, a negative regulator of NF-kappaB, in RAW 264.7 macrophages. J. Nanosci. Nanotechnol. 15, 6509–6515.
Kim, Y.S., Gupta Vallur, P., Phaëton, R., Mythreye, K., Hempel, N., 2017. Insights into the dichotomous regulation of SOD2 in cancer. Antioxidants 6, 86.
Krishnamoorthy, K., Premanathan, M., Veerapandian, M., Kim, S.J., 2014. Nanostructured molybdenum oxide-based antibacterial paint: effective growth inhibition of various pathogenic bacteria. Nanotechnology 25.
Krishnamoorthy, K., Veerapandian, M., Yun, K., Kim, S.J., 2013. New function of molybdenum trioxide nanoplates: Toxicity towards pathogenic bacteria through membrane stress. Colloid Surf. B 112, 521–524.
Lawrence, T., 2009. The nuclear factor NF-kappaB pathway in inflammation. Cold Spring Harb. Perspect. Biol. 1, a001651.
Lehmann, S.G., Toybou, D., Pradas del Real, A.-E., Arndt, D., Tagmount, A., Viau, M., Safi, M., Pacureanu, A., Cloetens, P., Bohic, S., Salomé, M., Castillo-Michel, H., Omaña-Sanz, B., Hofmann, A., Vulpe, C., Simonato, J.-P., Celle, C., Charlet, L., Gilbert, B., 2019. Crumpling of silver nanowires by endolysosomes strongly reduces toxicity. Proc. Natl. Acad. Sci. 116, 14893.
Liu, Y., Hardie, J., Zhang, X., Rotello, V.M., 2017. Effects of engineered nanoparticles on the innate immune system. Semin. Immunol. 34, 25–32.
Livak, K.J., Schmittgen, T.D., 2001. Analysis of relative gene expression data using real-time quantitative PCR and the 2(T)(-Delta Delta C) method. Methods 25, 402–408.
Lopes, E., Picarra, S., Almeida, P.L., de Lencastre, H., Aires-de-Sousa, M., 2018. Bactericidal efficacy of molybdenum oxide nanoparticles against antimicrobial-resistant pathogens. J. Med. Microbiol. 67, 1042–1046.
Marano, F., Hussain, S., Rodrigues-Lima, F., Baeza-Squiban, A., Boland, S., 2011. Nanoparticles: molecular targets and cell signalling. Arch. Toxicol. 85, 733–741.
Miao, L., St Clair, D.K., 2009. Regulation of superoxide dismutase genes: implications in disease. Free Radic. Biol. Med. 47, 344–356.
Mosmann, T., 1983. Rapid colorimetric assay for cellular growth and survival - application to proliferation and cyto-toxicity assays. J. Immunol. Methods 65, 55–63.
Mrzel, A., Remskar, M., Jesih, A., Virsek, M., 2011. Process for the Synthesis of Nanotubes and Fullerene-Like Nanostructures of Transition Metal Dichalcogenides, Quasi One-Dimensional Structures of Transition Metals and Oxides of Transition Metals. Inst & Ldquo Jo Hacek Over Z Ef Stefan & Rdquo, US.
Niska, K., Pyszka, K., Tukaj, C., Wozniak, M., Radomski, M.W., Inkielewicz-Stepniak, I., 2015. Titanium dioxide nanoparticles enhance production of superoxide anion and alter the antioxidant system in human osteoblast cells. Int. J. Nanomed. 10, 1095–1107.
Perez, D.M., Papay, R.S., Shi, T., 2009. alpha1-Adrenergic receptor stimulates interleukin-6 expression and secretion through both mRNA stability and transcriptional regulation: involvement of p38 mitogen-activated protein kinase and nuclear factor-kappaB. Mol. Pharmacol. 76, 144–152.
Picarra, S., Lopes, E., Almeida, P.L., de Lencastre, H., Aires-de-Sousa, M., 2019. Novel coating containing molybdenum oxide nanoparticles to reduce Staphylococcus aureus contamination on inanimate surfaces. PLoS One 14.
Raj, S., Jose, S., Sumod, U.S., Sabitha, M., 2012. Nanotechnology in cosmetics: opportunities and challenges. J. Pharm. Bioallied Sci. 4, 186–193.
Rusydi, A.F., 2018. Correlation between conductivity and total dissolved solid in various type of water: a review. IOP Conf. Ser. Earth Environ. 118.
Safi, M., Yan, M., Guedeau-Boudeville, M.A., Conjeaud, H., Garnier-Thibaud, V., Boggetto, N., Baeza-Squiban, A., Niedergang, F., Averbeck, D., Berret, J.F., 2011. Interactions between magnetic nanowires and living cells: uptake, toxicity, and degradation. ACS Nano 5, 5354–5364.
Sakai, N., Wada, T., Furuichi, K., Iwata, Y., Yoshimoto, K., Kitagawa, K., Kokubo, S., Kobayashi, M., Takeda, S.i., Kida, H., Kobayashi, K.i., Mukaida, N., Matsushima, K., Yokoyama, H., 2002. p38 MAPK phosphorylation and NF-κB activation in human crescentic glomerulonephritis. Nephrol. Dial. Transpl. 17, 998–1004.
Sivan, S.K., Padinjareveetil, A.K.K., Padil, V.V.T., Pilankatta, R., George, B., Senan, C., Cernik, M., Varma, R.S., 2019. Greener assembling of MoO3 nanoparticles supported on gum arabic: cytotoxic effects and catalytic efficacy towards reduction of p-nitrophenol. Clean Technol. Environ. 21, 1549–1561.
Sugawara, T., Gallucci, R.M., Simeonova, P.P., Luster, M.I., 2001. Regulation and role of interleukin 6 in wounded human epithelial keratinocytes. Cytokine 15, 328–336.
Varlec, A., Arcon, D., Skapin, S.D., Remskar, M., 2016. Oxygen deficiency in MoO_3 polycrystalline nanowires and nanotubes. Mater. Chem. Phys. 170, 154–161.
Wan, R., Mo, Y., Feng, L., Chien, S., Tollerud, D.J., Zhang, Q., 2012. DNA damage caused by metal nanoparticles: involvement of oxidative stress and activation of ATM. Chem. Res. Toxicol. 25, 1402–1411.
Wang, L.L., Hu, C., Shao, L.Q., 2017. The antimicrobial activity of nanoparticles: present situation and prospects for the future. Int. J. Nanomed. 12, 1227–1249.
Zimmerman, J.F., Parameswaran, R., Murray, G., 2016. Cellular uptake and dynamics of unlabeled freestanding silicon nanowires. Sci. Adv. 2, e1601039.
Zollfrank, C., Gutbrod, K., Wechsler, P., Guggenbichler, J.P., 2012. Antimicrobial activity of transition metal acid MoO_3 prevents microbial growth on material surfaces. Mater. Sci. Eng. C-Mater. 32, 47–54.